NANO LETTERS

pubs.acs.org/NanoLett

Letter

Spontaneous Polarity Flipping in a 2D Heterobilayer Induced by Fluctuating Interfacial Carrier Flows

Hua Li, Honglei Li, Xingzhi Wang, Yufeng Nie, Cheng Liu, Yu Dai, Jinyang Ling, Mengning Ding, Xi Ling, Daiqian Xie, Ning Lu, Changjin Wan, Qihua Xiong,* and Weigao Xu*

Cite This: *Nano Lett.* 2021, 21, 6773−6780

Read Online

ACCESS | Metrics & More | Article Recommendations | Supporting Information

ABSTRACT: Polarity often refers to the charge carrier type of a semiconductor or the charging state of a functional group, generally dominating their functionality and performance. Herein we uncover a spontaneous and stochastic polarity-flipping phenomenon in monolayer WSe_2, which randomly switches between the *n*-type and *p*-type states and is essentially triggered by fluctuating carrier flows from or to the adjacent WS_2 monolayer. We have traced such fluctuating carrier flows by interfacial photocurrent measurements in a zero-bias two-terminal device. Such polarity flipping results in switching between the negative and positive correlations between the emission intensities of WS_2 and WSe_2 in the heterobilayer, which is further well-controlled by the electrostatic gate-tuning experiments in a capacitor-structure device. Our work not only demonstrates giant and intermittent carrier flows through long-range coupling in 2D heterostructures and a consequent spontaneous polarity flipping phenomenon but also provides a two-emitter system with a switchable correlation sign that could project future applications in optical logic devices.

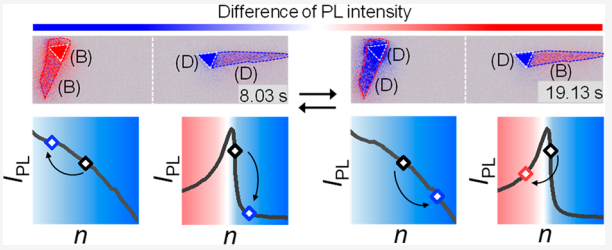

KEYWORDS: *Polarity flipping, fluorescence blinking, charge transfer, 2D materials*

INTRODUCTION

The polarity of a chemical group refers to the charging state of its center atom.[1−4] The inversion of polarity allows a certain chemical group that is a nucleophile (electrophile) to be an electrophile (nucleophile). Such polarity reversal strategies via either a classical chemical approach[1,5−7] or electrostatic tuning[8,9] are important in synthetic chemistry. In semiconductors, polarity usually refers to the doping state (either *n*-type or *p*-type),[10] which is key to its applications in various electronic and optoelectronic devices.[11−13] Compared to that of bulk materials, the polarity of two-dimensional (2D) crystals can be readily tuned due to the large surface-to-volume ratio by controlling the dopants and charge carriers, such as surface functionalization,[6] atomic substitution,[7] and electrostatic tuning with a gate voltage.[9,14,15]

2D van der Waals (vdW) heterostructures, which consist of vertically stacked diverse monolayers, have offered an excellent platform for exploring, utilizing, and tailoring interfacial interactions.[16−19] Pioneering works have reported various interface-induced features, such as moiré excitons,[20−23] the fractal quantum Hall effect,[18] and superconductivity.[24] In contrast to above works that usually require a strong interfacial coupling, fluctuations of the interlayer charge carrier flows and the consequent fluorescence blinking effect have been observed in weakly coupled 2D semiconductor heterostructures.[25,26] According to the Marcus theory, carrier transfer is generally difficult in such long-range coupled heterobilayers.[27,28] In this work, we directly captured the fluctuations of interlayer carrier flows in a zero-bias heterobilayer device with the fluorescence blinking effect. We also report a dynamic polarity flipping phenomenon of monolayer WSe_2 surface, which is induced by cascaded interlayer carrier flows between constituents in a WSe_2/WS_2 heterobilayer. Besides physical insights on the long-range interactions at the interface, this work also provides a degree of freedom in the future design and application of novel quantum materials and devices.

RESULTS AND DISCUSSION

Correlated Fluorescence Blinking: The Missing Part. The investigated WSe_2/WS_2 heterobilayer was prepared by stacking two corresponding monolayers via aligned transfer.[25] The monolayer characteristics of each component and their weak coupling state can be confirmed through spectroscopic methods. Both the vibrational fingerprints in Raman scattering and fluorescence emission features exhibit barely any shift in the heterobilayer, which is distinct from a strongly coupled (*i.e.*, quenched in fluorescence) heterobilayer (Supporting Informa-

Received: April 5, 2021
Revised: August 4, 2021
Published: August 12, 2021

https://doi.org/10.1021/acs.nanolett.1c01356
Nano Lett. 2021, 21, 6773−6780

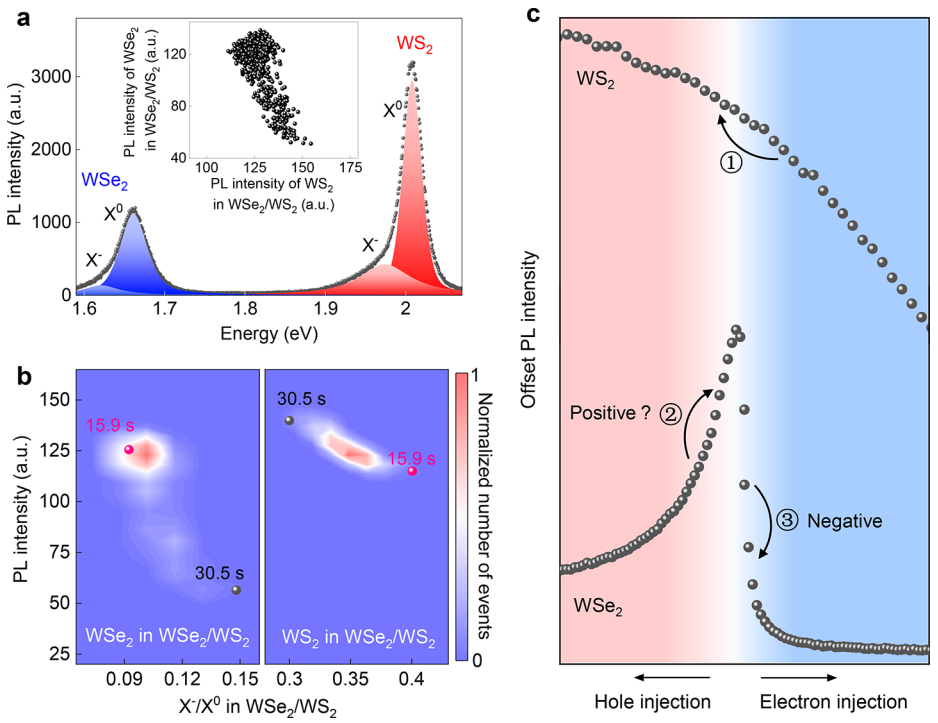

Figure 1. Correlated fluorescence blinking in a WSe_2/WS_2 emitter pair and the missing part. (a) Typical photoluminescence (PL) spectrum of the WSe_2/WS_2 heterobilayer (optical image shown in Supporting Information Figure S3a), with 532 nm laser excitation. Inset shows the statistical state distribution of PL intensities of WS_2 and WSe_2 according to the time profile in Figure S3b. (b) Statistical state distribution of intensity versus the trion/exciton ratio (X^-/X^0), corresponding to time traces in Figure S3b. The two sets of correlated points at two moments are marked with red (t = 15.9 s) and black (t = 30.5 s) for clarity. (c) Illustration of a hypothetical mechanism for the positively and negatively correlated emission of 2D emitters associated with their polarities. For electron transfer process 1 from WS_2 to WSe_2, the ambipolar WSe_2 could become either brighter (process 2 at the left branch, *i.e.*, the "missing part") or darker (process 3 at the right branch) than the initial state. Gate-dependent PL emission intensities of WSe_2 and WS_2 monolayers are adapted from measurements in Figure S2.

tion Section 1 and Figure S1). We conducted gate-dependent photoluminescence (PL) measurements[9,14] to examine the doping state of the WS_2 and WSe_2 monolayers, which were excited by a 532 nm laser (3 μW) at room temperature and in atmosphere. As the result, the PL intensity monotonically decreases with the increasing trion-to-exciton ratio ($X^{\pm}/X^0$), which could be utilized to indirectly reflect the doping level (Supporting Information Section 2 and Figure S2). The gate voltage-dependent (V_g) emission intensity of monolayer WSe_2 shows an apparent ambipolar behavior, which is n-type at a positive V_g and p-type at a relatively large negative V_g. The charge neutrality point (CNP) with a maximum PL intensity at $V_g = -0.65$ V indicates a slight n-type nature of the pristine WSe_2 monolayer. In contrast, the investigated WS_2 monolayer stays n-type at the full range of the applied V_g (from −40 to +40 V), indicating a much heavier n-type doping compared to that WSe_2; this is mainly due to the sulfur vacancies.[29]

The typical emission spectrum of an n-WSe_2/n-WS_2 (the prefix "n-" or "p-" means n-type or p-type, respectively) heterobilayer in Figure 1a shows the characteristic emission peaks of WS_2 located at ∼2.02 eV (614 nm) and those of WSe_2 located at ∼1.66 eV (747 nm). From a batch analysis of a spectral time profile (Supporting Information Section 3 and Figure S3), the emission from each material includes the contribution of X^0 and X^-. The emission intensity from each component clearly fluctuates with time, indicating a distinct fluorescence blinking effect (Figure S3b).[25,26] Moreover, the emission intensities of two components show a negative correlation (inset of Figure 1a), with a Pearson's correlation coefficient $\rho = -0.72$ (Supporting Information Section 4). In a statistical state distribution analysis (Figure 1b), we found that both WSe_2 and WS_2 exhibit negative correlations between the total intensity and the X^-/X^0 ratio. For example, at t = 30.5 s, WSe_2 is in a dark state with a higher X^-/X^0 ratio, while WS_2 is in a bright state with a lower X^-/X^0 ratio. This should correspond to an electron transfer event from n-WS_2 to n-WSe_2 (or hole transfer in the opposite direction), which is consistent with the above-mentioned gate-dependent PL experiments of monolayers (Supporting Information Section 2 and Figure S2). The PL intensity variation of each constituent seems to follow a "charge neutrality principle" (Supporting Information Section 5 and Figure S4), where the strongest emission occurs at the CNP with the lowest $X^{\pm}/X^0$ ratio. With this hypothesis, as illustrated in Figure 1c, one may also expect to observe positively correlated emissions besides the above-mentioned negative correlations. Specifically, when electrons are transferred from WS_2 to WSe_2 (process 1), the ambipolar WSe_2 could become either brighter (process 2 at the left branch, *i.e.*, the "missing part"), or darker than the initial state (process 3 at the right branch).

Observation of the Spontaneous Polarity Flipping Phenomenon. In the second part of our experiment, we performed a time-dependent dual-channel fluorescence imaging measurement on an n-WSe_2/n-WS_2 heterobilayer (Supporting Information Section 6.1 and Figure S5). Unlike the point-excited fluorescence spectroscopy measurement in Figure 1, dual-channel fluorescence imaging with homogeneous illumination over the whole sample allows the separate extraction of spatially resolved time-dependent grayscale intensities of

https://doi.org/10.1021/acs.nanolett.1c01356
Nano Lett. 2021, 21, 6773−6780

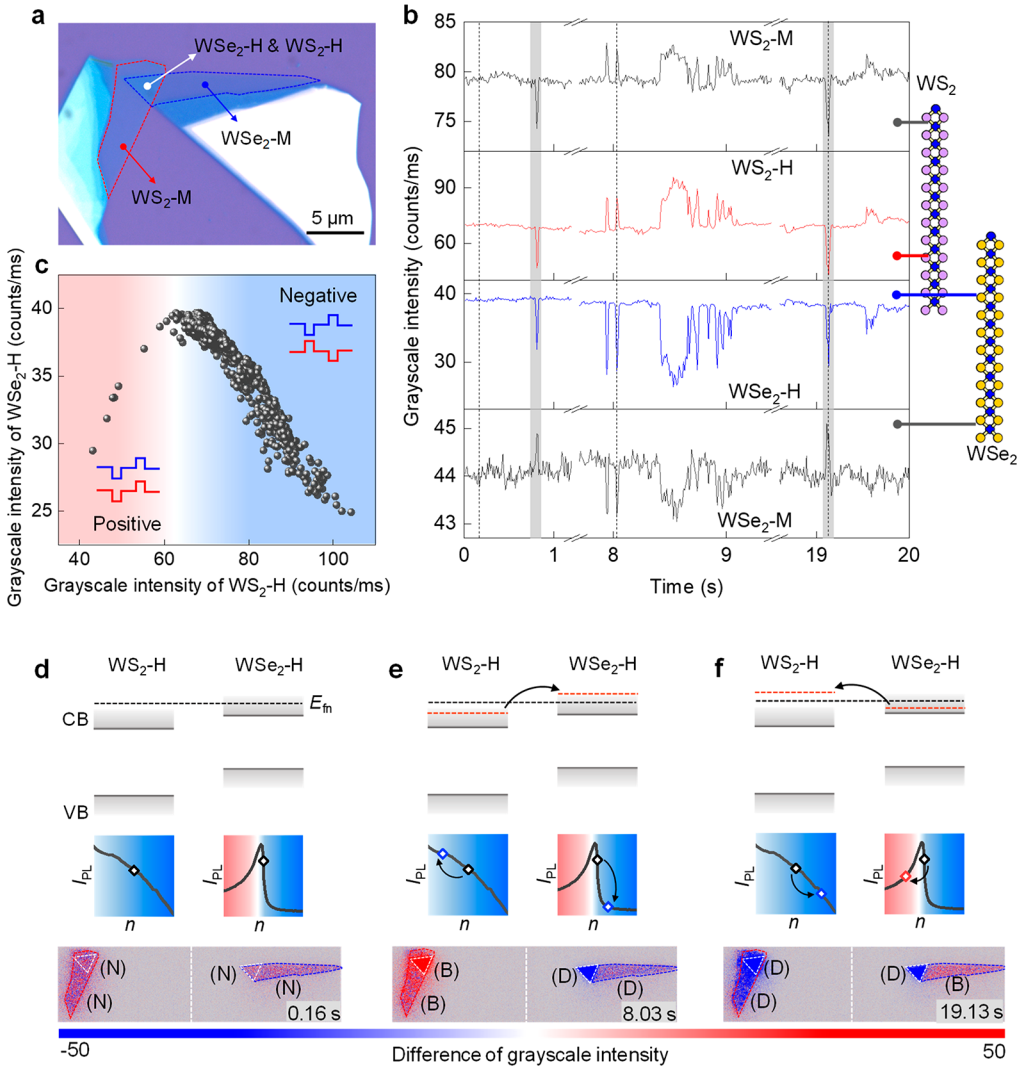

Figure 2. Polarity flipping in an *n*-WSe_2/*n*-WS_2 heterobilayer. (a) Optical image of the *n*-WSe_2/*n*-WS_2 heterobilayer, including the heterobilayer region and two monolayer regions. (b) Time traces of grayscale intensities of the four regions in the *n*-WS_2/*n*-WSe_2 heterobilayer. The curves are for the WS_2 fluorescence in both the monolayer (WS_2−M) and the heterobilayer (WS_2−H) regions and the WSe_2 fluorescence in both the heterobilayer (WSe_2−H) and the monolayer (WSe_2−M) regions from top to bottom, as illustrated in the crystal structure on the right side. Two vertical shadow areas indicate the moments when the $n \rightarrow p \rightarrow n$ polarity flipping happens. (c) Statistical state distribution of the relation between the fluorescence intensities of WS_2 and WSe_2 in the heterobilayer region, which shows positive and negative correlation. (d) The quasi-steady-state illuminated by consistent light. The dashed black line indicates the electron quasi-Fermi level (E_{fn}). (e) A polarity-remained blink event starting from the quasi-steady state in which electrons are transferred from WS_2−H to WSe_2−H, resulting in the increased fluorescence of WS_2−H and the decreased fluorescence of WSe_2−H. (f) A polarity flip event starting from the quasi-steady state with electrons transferring from WSe_2−H to WS_2−H in which WSe_2−H flips from *n*-type to *p*-type. CB and VB represent conduction band and the valence band, respectively. The dashed red line indicates E_{fn} at deviated states. Sets of black arrows indicate the transfer direction. $I_{PL} \sim n$ curves (simplified figures of the gate-dependent fluorescence in Supporting Information Figure S2) show the emission intensity (I_{PL}) variation with the injection (outflow) of carriers (n). The blue and red fillings correspond to the *n*-type and *p*-type of each monolayer material, respectively. Bottom panels of panels d−f show the representative difference fluorescence images at the three moments labeled by dashed black lines in panel b, where the WS_2 emission is shown on the left channel and the WSe_2 emission is shown on the right channel. Specifically, a neutral state at 0.16 s, a negative correlation with the brightened WS_2 and dimmed WSe_2 emission at 8.03 s, and an anomalous (positive correlation) state at 19.13 s. N, B, and D indicate neutral, bright, and dark states, respectively.

different regions. For clarity, we labeled the WS_2 and WSe_2 components in the heterobilayer region as WS_2−H and WSe_2−H and the two connected bare monolayer regions as WS_2-M and WSe_2-M (Figure 2a). We plotted the grayscale intensities of WS_2−H and WSe_2−H as a function of time (red and blue curves, respectively, in Figure 2b). The time traces of the two components at the heterojunction region do have moments that exhibit a blinking effect with a negative correlation. Remarkably, we can also unambiguously observe some moments when positive correlations occur between the emissions from WS_2−H and WSe_2−H, as vertically shadowed in Figure 2b. More intuitively, the correlation diagram of the fluorescence intensity of WS_2−H and WSe_2−H exhibits a "Λ" shape, indicating two distinct types of correlation (Figure 2c). Besides the right branch with a negative slope indicating a negative correlation, the left branch with a positive slope indeed manifests the events with a positive correlation. We refer to such moments as "anomalous events" since they appear to violate the aforementioned "charge neutrality principle" in an *n*-*n*-type heterostructure (Supporting Information Section 5), while

https://doi.org/10.1021/acs.nanolett.1c01356
Nano Lett. 2021, 21, 6773−6780

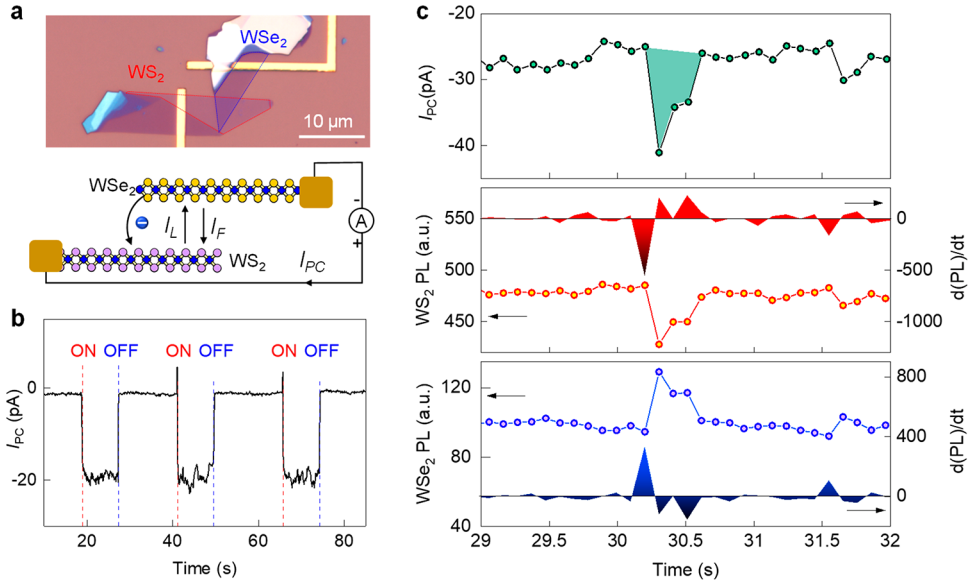

Figure 3. Capture of interfacial photocurrent in a blinking WSe_2/WS_2 circuit at zero bias. (a) Optical image and schematic illustration of the two-terminal device, where I_L and I_F represent the photogenerated current and the photovoltage-induced forward current, respectively. The negative photocurrent (I_{PC}) implies that electrons are transferred from WSe_2 to WS_2. (b) The photoresponse of *n*-WSe_2/*n*-WS_2 in a circuit with and without laser illumination under zero bias voltage. An apparent repeatable I_{PC} appears when the laser is on. (c) Synchronous time-profile measurement of I_{PC} together with PL emissions from WS_2 and WSe_2, from the top panel to the bottom panel, respectively. In the top panel at $t = 30.3$ s, the green integrated area gives an extra flow of 2.1×10^7 electrons, which is about three orders of magnitude larger than the fluctuation event estimated in Figure 3 and Supporting Information Figure S7 without a circuit (4.0×10^4 electrons). The filling patterns in the middle and bottom panels are the differential analyses calculated from the corresponding time traces of PL intensities, where the positive and negative peaks reflect the direction of charge accumulation, *i.e.*, the red negative peak and the blue positive peak indicate an electron transfer process of WSe_2 to WS_2 and vice versa, respectively.

those negatively correlated moments are referred to as "normal events". More intuitively, difference fluorescence images present three typical moments of a neutral state at 0.16 s, a negative correlation at 8.03 s, and a positive correlation at 19.13 s during the same acquisition, which are shown in the bottom panels in Figure 2d–f, respectively (each frame was subtracted by the first quasi-steady state image, and full-frame images are included in the Supporting Video, two anomalous events at 0.81 s and 19.13 s, as well as one normal event at 8.03 s, are paused for ~3 s for clarity).

To figure out the underlying mechanism of the anomalous events, we investigated the PL intensities of WS_2–M and WSe_2–M over the same period (black curves in Figure 2b). The PL intensities of the monolayer regions also fluctuate with time, with a much smaller amplitude and mainly with a positive correlation compared to that of the same component in the heterobilayer region. This should originate from the redistribution of carriers within one monolayer, *i.e.*, intralayer carrier transfer triggered by an interlayer carrier transfer event (Supporting Information Figure S6). In contrast to the constant intralayer positive correlation of emissions from WS_2 (*i.e.*, between WS_2–M and WS_2–H), the intralayer correlation of emissions from WSe_2 (*i.e.*, between WSe_2–M and WSe_2–H) changes from positive to negative at the vertically shadowed anomalous moments (Figure 2b). Consistently and more intuitively, opposite intralayer correlations of the WSe_2 emission can be well resolved in the difference images shown in Figure 2e and f, *e.g.*, positive at 8.03 s and negative at 19.13 s, respectively. The opposite responses of WSe_2–H and WSe_2–M to the same-type charge carrier transfer imply their opposite polarities (Supporting Information Figure S6c). To be noted, the negative intralayer correlation of WSe_2 unambiguously excludes the possibility that the anomalous positive interlayer correlation is caused by some disturbing factors, such as vibrations from the environments or charge carrier loss to a third component such as a substrate.

The fluorescence blinking effect in a 2D system can be explained with an intermittent interlayer carrier transfer (IICT) model.[25] Here we take electron transfer as an example to describe the interfacial carrier transfer. When illuminated by photons, the heterobilayer system is in a nonequilibrium state where electrons in each component are continuously excited to the conduction band (CB) and leave holes in the valence band (VB). In this case, both quasi-Fermi levels of the electrons (E_{fn}) of the constituents go up, and their relative position determines the direction of the net interlayer electron transfer in a heterobilayer. Besides the fluctuating moments, both WSe_2–H and WS_2–H dwell at a balanced state with a stable emission (Figure 2b). This indicates that the system tends to reach a quasi-steady state, where the electron quasi-Fermi levels of two components match with each other (Figure 2d).

In 2D vdW semiconductor heterostructures, the ultrafast dynamics of interlayer electron transfer[25,30] and energy transfer[31,32] have attracted tremendous experimental and theoretical efforts.[28] In recent theoretical investigations, interfacial carrier transfer was proposed to be facilitated by interlayer electronic state mixing[33,34] and phonon scattering.[35] In our weakly coupled heterobilayer, the interfacial fluctuations are possibly enhanced by the limited and intermittent overlap of electronic wave functions across the heterojunctions. Consequently, the system is going to deviate from the quasi-steady state, resulting in a carrier density variation and a fluctuation of the emission intensity in each component. To be noted, WSe_2–H shows almost the strongest PL emission at the "steady-state" moments, suggesting that it is near intrinsic at quasi-steady state. The negative correlation with the enhanced WS_2–H emission

https://doi.org/10.1021/acs.nanolett.1c01356
Nano Lett. 2021, 21, 6773–6780

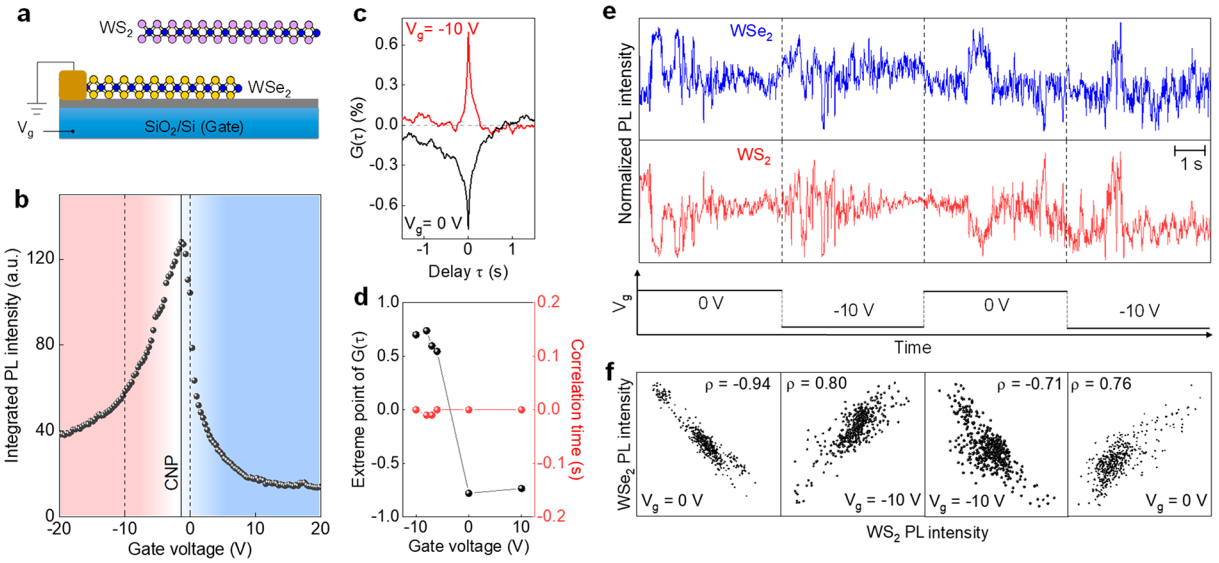

Figure 4. Electrostatic control of the polarity reversal and switchable fluorescence correlation in the WSe_2/WS_2 heterobilayer. (a) Schematic illustration of the back-gated WSe_2/WS_2 device. (b) Fluorescence intensity of WSe_2 in WSe_2/WS_2 as a function of the back gate voltage, indicating its *n*-type nature without applying the back-gate voltage. Black dashed lines indicate the positions of the gate voltage applied, and the solid black line marks the charge neutrality point (CNP) at −1.32 V. (c) $G(\tau)$ calculated from the time-trace data at $V_g = 0$ and −10 V, indicating a prominent negative correlation (0 V) and a positive correlation (−10 V) at time zero, respectively. (d) The extreme points of $G(\tau)$ and the correlation time at different V_g values. (e) Time traces of baselined and normalized grayscale intensities of WSe_2 and WS_2 at the heterostructure region under a square-wave gate voltage. The WSe_2 constituent is originally *n*-type ($V_g = 0$ V) and becomes *p*-type when $V_g = -10$ V. (f) Correlation diagrams of the correlated emission of WS_2 and WSe_2 in panel e. The calculated Pearson's correlation coefficients are also presented.

and the quenched WSe_2−H emission is due to an electron transfer process from WS_2−H to WSe_2−H (Figure 2e). In contrast, when electrons transfer from WSe_2−H to WS_2−H, negative-correlated events with a slightly enhanced WSe_2−H emission and a quenched WS_2−H emission are observable (Figure 2b). However, we also see the more prominent anomalous events (*i.e.*, a clear positive correlation with quenched WS_2−H and WSe_2−H emissions), which predict the probable $n \rightarrow p$ polarity flipping events in WSe_2−H. Specifically, when the cascaded transfer of electrons (exceeding a threshold amount) from WSe_2−H to WS_2−H occurs, the extra charge densities of both materials (*i.e.*, the electron density of WS_2−H and the hole density of WSe_2−H) increase, resulting in a positive correlation with the darkened emissions of both WSe_2−H and WS_2−H (red and blue squares in the $I_{PL} \sim n$ diagrams in the bottom of Figure 2f). At the same time, WSe_2−M will passively transport much fewer electrons to WSe_2−H, which is not enough to reverse the polarity of WSe_2−M and brighten its PL emission. According to the gate-dependent PL profile and the grayscale change in the fluorescence imaging, we can estimate the number of electrons involved in a polarity flipping event. For example, at $t = 19.13$ s, we obtained a carrier flow of $\sim 6.8 \times 10^{11}$ cm^{-2} (an equivalent amount of 4.0×10^4 electrons with a sample size of 5.9 μm^2), which is enough to overwhelm the initial background carrier density of $\sim 5.1 \times 10^{10}$ cm^{-2} (Supporting Information Section 6.3 and Figure S7). Such a polarity-flipped state is away from quasi-steady state and usually flips back quickly, resulting an $n \rightarrow p \rightarrow n$ flipping cycle.

Direct Capture of Interlayer Carrier Flows. Such rapid and drastic charge transfer shall result a measurable current even without a bias; thus, we further devised and conducted the photocurrent measurements to detect the interfacial carrier transfer under a zero bias (Figure 3a). As can be seen in Figure 3b, a pronounced negative photocurrent around −19 pA was detected under the illumination of a 532 nm laser (power of 180 μW and spot size ~2 μm). This pronounced current indicates an ordered interfacial electron flow from WSe_2 to WS_2 at around 1.2×10^8 electrons per second. The system finally reaches a quasi-steady state, with balanced photocurrent (I_{PC}) in the forms of $I_{PC} = I_L - I_F$, where I_L and I_F are the photogenerated current and photovoltage-induced forward current, respectively (Figure 3a). Furthermore, in an *in situ* time profile of the optoelectronic measurement, I_{PC} exhibits a synchronous fluctuation as the PL of the two constituents (Figure 3c). For example, an I_{PC} increase at $t = 30.3$ s indicates an outflow of electrons from WSe_2 to WS_2, resulting in brightened WSe_2 emissions (polarity not reversed) and darkened WS_2 emissions. The well-synchronized photocurrent response to the fluctuation pace of the PL indicates an interlayer carrier transfer rather than energy transfer in our cases. The integrated area shadowed by green gives an extra flow of 2.1×10^7 electrons (Supporting Information Section 7.1 and Figure S8), which is orders of magnitude larger than the estimated value of 1.3×10^3 calculated from the PL fluctuation of WSe_2 in Figure 3c and that of 4.0×10^4 for the case of $t = 19.13$ s in Figure 2. To clarify this difference it shall be noted that the PL intensities are associated with the charge accumulation. In a circuit device, as illustrated in Figure 3a, I_F is the factor that finally affects the carrier accumulation and PL emission, while I_{PC} represents the flowing carriers in the circuit, which are not accumulated at the interface.

On-Demand Access to Negative and Positive Fluorescence Correlations. To confirm the relation between correlation switching and the polarity flipping of WSe_2 and to obtain the on-demand switching of correlated emitters, we conducted a gate-dependent study on the fluorescence blinking of a heterobilayer in a capacitor structure (Figure 4a). The PL intensity of WSe_2 at the heterobilayer region reaches a maximum when $V_g = -1.32$ V, indicating its slight *n*-type nature when $V_g = 0$ (Figure 4b). When $V_g = -10$ V, WSe_2 can be tuned to the *p*-type via injecting holes. Therefore, the WSe_2 layer can be

https://doi.org/10.1021/acs.nanolett.1c01356
Nano Lett. 2021, 21, 6773−6780

electrostatically tuned to the *n*-type and the *p*-type by setting V_g as 0 and −10 V, respectively, while the adjacent WS_2 layer remains *n*-type (Supporting Information Figure S2b). The cross-correlation functions $G(\tau)$ of two components at different V_g levels (0 and −10 V) are calculated (Figure 4c), which is defined as

$$G(\tau) = \frac{\langle \partial I_{WS_2}(t) \cdot \partial I_{WSe_2}(t+\tau) \rangle}{\langle I_{WS_2}(t) \rangle \cdot \langle I_{WSe_2}(t) \rangle} = \frac{\langle I_{WS_2}(t) \cdot I_{WSe_2}(t+\tau) \rangle}{\langle I_{WS_2}(t) \rangle \cdot \langle I_{WSe_2}(t) \rangle} - 1$$

where $G(\tau)$ is the cross-correlation function, I is the signal intensity with the largest occurrence in the signal-level distribution, t is time, τ refers to the time delay of the correlation. We took the emission intensities from the two components at time t. The $G(\tau)$ dip at the zero-time delay suggests a prominent and immediate negative correlation between the WS_2 and WSe_2 components of the emitter pair as $V_g = 0$, while the $G(\tau)$ rise at the zero-time delay indicates an immediate positive correlation when a negative $V_g = -10$ V is applied (Figure 4c). We have carried out systematic electrostatic gating experiments from 10 to −10 V on the same device, which suggest that the *n*-type to *p*-type transition occurs between −6 to 0 V (Figure 4d, black curve). Interestingly and more specifically, we found that the gate-dependent blinking amplitude follows well with the first derivative (absolute value) of the gate-dependent PL intensity curve of WSe_2, while the blinking frequency is almost independent of the value of V_g (Supporting Information Section 7.3 and Figures S10 and S11). In our experimental conditions, the correlation time was found to remain constant at different V_g levels (Figure 4d and Supporting Information Figure S12).

To be more intuitional and take 0 and −10 V as examples, Figure 4e shows two typical electrostatic gating cycles during a continuous *in situ* optoelectronic measurement. At $V_g = 0$ V (*i.e.*, *n*-*n*-type), the PL intensities of the two components are negatively correlated, whereas their correlation becomes positive at $V_g = -10$ V (*i.e.*, *p*-*n*-type). The Pearson's correlation plots further prove that the correlation of the blinking is negative in the *n*-*n*-structure and positive in the *p*-*n*-structure (Figure 4f).

To investigate the universality of polarity flipping, we used a slightly doped *p*-WSe_2 monolayer instead of *n*-WSe_2 to form a *p*-WSe_2/*n*-WS_2 heterobilayer. Interestingly, we found a positive correlation-dominated background together with much more frequent anomalous negative correlation events and thus more electron transfer events from WS_2 to WSe_2, which is possibly due to a higher density of states of electrons in WS_2. This result indicates random flipping $p \rightarrow n \rightarrow p$ cycles in contrast to the $n \rightarrow p \rightarrow n$ flipping cycles observed in *n*-WS_2/*n*-WSe_2. Detailed results and discussions are presented in Supporting Information Section 8 and Figures S13−15.

CONCLUSION

In summary, we have demonstrated a polarity flipping phenomenon for an ambipolar 2D semiconductor in a weakly coupled heterobilayer, which is induced by spontaneous and stochastic fluctuating interlayer carrier flows overwhelming the initial background carriers. Systematic optical and optoelectronic studies have been implemented to trace and quantify such giant and intermittent carrier flows. The polarity flipping of the semiconductor provides a surface with a fluctuating charging state, which is inspiring to explore in many scenarios, such as reversable adsorption and desorption or even as novel catalysts with a switchable chemical affinity. This work not only achieves substantial insights to the unique charge transfer behavior in the correlated emitter pair but also clarifies their in-depth synergistic mechanism (either positively or negatively). We believe that our findings will benefit the bottom-up design of hierarchical materials and optoelectronic devices with desirable functionalities.

MATERIALS AND METHODS

Sample Preparation. All pristine and doped crystals used here were purchased from 2D Semiconductors. We used mechanical exfoliation to obtain high-quality monolayer materials, which were further assembled into heterobilayers via the aligned dry transfer method.[25] All measurements were implemented at room temperature and in an ambient atmosphere if not otherwise noted.

Optical Spectroscopy Measurements. Emission spectra were measured on a Horiba HR Evolution spectrometer. To collect the fluorescence spectra from WS_2 and WSe_2 simultaneously, we used a 100 lines per millimeter grating with a single window span size of 189 nm centered at 689.5 nm. The excitation light was a 532 nm continuous wave laser (3 μW, spot size ∼1 μm). Time profiles of the emission spectra were collected every 100 ms, with a time interval of ∼0.26 ms. For the analysis of time-dependent emissions from recombination of excitons and trions, we used Labspec6 software for the batch fitting process and obtained integrated intensity profiles of both neutral excitons and trions.

Dynamically Correlated Fluorescence Imaging. The samples were excited by an Olympus U-HGLGPS lamp (130 W output) after being passed through a 530/40 nm band-pass filter. The excitation power was ∼3.34 mW when arriving at the sample. The emission of the sample was reflected by a 570 nm long-pass dichroic mirror and divided into two beams by a 50:50 beam splitter. Band-pass filters of 618/50 and 747/33 nm (from Semrock) were used to selectively extract emissions from WS_2 and WSe_2, respectively. A schematic optical path diagram is shown in Supporting Information Figure S5a. Dynamic variations in the fluorescence image were recorded by a high-speed S-CMOS camera (Teledyne Photometrics Prime 95B) with a speed of 100 frames per second and a negligible time interval (∼10 ms exposure time for each frame). The time traces were extracted from the grayscale value of regions of interest in each frame. Difference fluorescence images were obtained by subtracting each frame by the first quasi-steady-state frame in ImageJ software.

***In Situ* Optoelectronic Measurements.** Electrodes were patterned on the SiO_2/Si substrates using standard electron-beam lithography and the metal evaporation of a titanium adhesion layer (20 nm) and gold (50 nm). Monolayer WSe_2 and WS_2 flakes prepared by mechanical exfoliation were transferred onto the patterned electrodes and assisted with a PDMS layer. We used point excitation with a 532 nm laser (180 μW power and ∼2 μm spot size) for the *in situ* photocurrent measurement and bright-filed illumination with the above-mentioned Olympus U-HGLGPS lamp for electrostatic gate-tuning measurements, respectively. All electrical measurements were implemented by a Keysight Technologies B2902A source meter. For electrostatic gating, the square-wave voltage of −10 V was applied on the device gate electrode with pulse width of 5 s, which was repeated five times with a cycle of 10 s. The hysteresis

https://doi.org/10.1021/acs.nanolett.1c01356
Nano Lett. 2021, 21, 6773−6780

background from adsorbents, which may affect the correlation analysis, was extracted for clarity, and raw data for the complete five cycles are shown in Supporting Information Figure S9.

■ ASSOCIATED CONTENT

Supporting Information

The Supporting Information is available free of charge at https://pubs.acs.org/doi/10.1021/acs.nanolett.1c01356.

Raman and PL spectra of strongly and weakly coupled heterobilayers, gate-dependent PL emission of WSe_2 and WS_2 monolayers, batch fitting of trions and neutral excitons in a spectral time profile, calculation of Pearson's correlation coefficients, discussions on the correlation sign for blinking heterojunctions with different combinations, dynamically correlated dual-channel fluorescence imaging, *in situ* optoelectronic study, and the $p \rightarrow n \rightarrow p$ type polarity flipping (PDF)

The difference fluorescence imaging profile that corresponds to data shown in Figure 2(MP4)

■ AUTHOR INFORMATION

Corresponding Authors

Qihua Xiong − *State Key Laboratory of Low Dimensional Quantum Physics, Department of Physics, Tsinghua University, Beijing 100084, China; Beijing Academy of Quantum Information Sciences, Beijing 100193, P.R. China; Beijing Innovation Center for Future Chips, Tsinghua University, Beijing 100084, P.R. China;* orcid.org/0000-0002-2555-4363; Email: qihua_xiong@tsinghua.edu.cn

Weigao Xu − *Key Laboratory of Mesoscopic Chemistry, School of Chemistry and Chemical Engineering, Nanjing University, Nanjing 210023, China;* orcid.org/0000-0002-3014-756X; Email: xuwg@nju.edu.cn

Authors

Hua Li − *Key Laboratory of Mesoscopic Chemistry, School of Chemistry and Chemical Engineering, Nanjing University, Nanjing 210023, China*

Honglei Li − *Key Laboratory of Mesoscopic Chemistry, School of Chemistry and Chemical Engineering, Nanjing University, Nanjing 210023, China*

Xingzhi Wang − *Department of Chemistry, Boston University, Boston, Massachusetts 02215, United States;* orcid.org/0000-0002-0929-854X

Yufeng Nie − *Key Laboratory of Mesoscopic Chemistry, School of Chemistry and Chemical Engineering, Nanjing University, Nanjing 210023, China*

Cheng Liu − *Key Laboratory of Mesoscopic Chemistry, School of Chemistry and Chemical Engineering, Nanjing University, Nanjing 210023, China*

Yu Dai − *Kuang Yaming Honors School, Nanjing University, Nanjing 210023, China*

Jinyang Ling − *Key Laboratory of Mesoscopic Chemistry, School of Chemistry and Chemical Engineering, Nanjing University, Nanjing 210023, China*

Mengning Ding − *Key Laboratory of Mesoscopic Chemistry, School of Chemistry and Chemical Engineering, Nanjing University, Nanjing 210023, China;* orcid.org/0000-0001-6581-3385

Xi Ling − *Department of Chemistry, Division of Materials Science and Engineering, and The Photonics Center, Boston University, Boston, Massachusetts 02215, United States*

Daiqian Xie − *Key Laboratory of Mesoscopic Chemistry, School of Chemistry and Chemical Engineering, Nanjing University, Nanjing 210023, China;* orcid.org/0000-0001-7185-7085

Ning Lu − *Anhui Province Key Laboratory of Optoelectric Materials Science and Technology, Anhui Laboratory of Molecule-Based Materials, The Key Laboratory of Functional Molecular Solids, Ministry of Education, Anhui Normal University, Anhui, Wuhu 241000, China;* orcid.org/0000-0003-2846-2496

Changjin Wan − *School of Electronic Science & Engineering and Collaborative Innovation Center of Advanced Microstructures, Nanjing University, Nanjing 210093, China*

Complete contact information is available at: https://pubs.acs.org/10.1021/acs.nanolett.1c01356

Author Contributions

W.X. conceived the initial idea with discussions with Q.X. W.X. and H.L. designed the experiments. H.L and X.W. fabricated the heterobilayers and performed the optical experiments. H.L.L., Y.N., C.L., and M.D. fabricated the capacitor structure devices. H.L.L., Y.N., J.L., and C.W. performed the electrostatic gate-tuning experiments. H.L., Y.D., X.W., X.L., N.L., D.X., W.X., and Q.X. contributed to experimental and theoretical analyses. H.L. collected and organized all experimental data. H.L., W.X., X.W., and Q.X. wrote the manuscript with input from all authors.

Notes

The authors declare no competing financial interest.

■ ACKNOWLEDGMENTS

We thank the Fundamental Research Funds for the Central Universities in China (020514380231 and 021014380177); the National Natural Science Foundation of China (21873048); the Natural Science Foundation of Jiangsu Province (BK20180319); the National Key R&D Program of China no. 2020YFA0406104, "Innovation & Entrepreneurship Talents Plan" of Jiangsu Province; the National Research Foundation for Youth Talents of China; and start-up funds from Nanjing University for financial support. N.L. acknowledges financial support from the Anhui Provincial Natural Science Foundation (no. 2008085QA33).

■ REFERENCES

(1) Seebach, D. Methods of reactivity umpolung. *Angew. Chem. Int. Ed. Engl.* **1979**, *18*, 239−336.

(2) Phillips, M. C.; Wang, M. W.; Swenberg, J. F.; McCaldin, J. O.; McGill, T. C. Proposal and verification of a new visible light emitter based on wide band gap II-VI semiconductors. *Appl. Phys. Lett.* **1992**, *61* (16), 1962−1964.

(3) Sacilotti, M.; Abraham, P.; Pitaval, M.; Ambri, M.; Benyattou, T.; Tabata, A.; Perez, M. A. G.; Motisuke, P.; Landers, R.; Morais, J.; Corre, A. L.; Loualiche, S. Structural and optical properties of AlInAs/InP and GaPSb/InP type II interfaces. *Can. J. Phys.* **1996**, *74* (5−6), 202−208.

(4) Chu, L.; Qing, F. L. Oxidative trifluoromethylation and trifluoromethylthiolation reactions using (trifluoromethyl)-trimethylsilane as a nucleophilic CF_3 source. *Acc. Chem. Res.* **2014**, *47* (5), 1513−1522.

(5) Wu, Y.; Hu, L.; Li, Z.; Deng, L. Catalytic asymmetric umpolung reactions of imines. *Nature* **2015**, *523* (7561), 445−450.

(6) Lei, S.; Wang, X.; Li, B.; Kang, J.; He, Y.; George, A.; Ge, L.; Gong, Y.; Dong, P.; Jin, Z.; Brunetto, G.; Chen, W.; Lin, Z.-T.; Baines, R.; Galvão, D. S.; Lou, J.; Barrera, E.; Banerjee, K.; Vajtai, R.; Ajayan, P. Surface functionalization of two-dimensional metal chalcogenides by Lewis acid−base chemistry. *Nat. Nanotechnol.* **2016**, *11* (5), 465−471.

(7) Gong, Y.; Yuan, H.; Wu, C. L.; Tang, P.; Yang, S.-Z.; Yang, A.; Li, G.; Liu, B.; van de Groep, J.; Brongersma, M. L.; Chisholm, M. F.; Zhang, S.-C.; Zhou, W.; Cui, Y. Spatially controlled doping of two-dimensional SnS_2 through intercalation for electronics. *Nat. Nanotechnol.* **2018**, *13* (4), 294−299.
(8) Heo, J.; Ahn, H.; Won, J.; Son, J. G.; Shon, H. K.; Lee, T. G.; Han, S. W.; Baik, M.-H. Electro-inductive effect: Electrodes as functional groups with tunable electronic properties. *Science* **2020**, *370* (6513), 214−219.
(9) Ross, J. S.; Wu, S. F.; Yu, H. Y.; Ghimire, N. J.; Jones, A. M.; Aivazian, G.; Yan, J. Q.; Mandrus, D. G.; Xiao, D.; Yao, W.; Xu, X. D. Electrical control of neutral and charged excitons in a monolayer semiconductor. *Nat. Commun.* **2013**, *4*, 1474.
(10) Pearson, G. L.; Bardeen, J. Electrical properties of pure silicon and silicon alloys containing boron and phosphorus. *Phys. Rev.* **1949**, *75* (5), 865−883.
(11) Kroemer, H. Theory of a wide-gap emitter for transistors. *Proc. IRE* **1957**, *45* (11), 1535−1537.
(12) Pospischil, A.; Furchi, M. M.; Mueller, T. Solar-energy conversion and light emission in an atomic monolayer p−n diode. *Nat. Nanotechnol.* **2014**, *9* (4), 257−261.
(13) Ross, J.; Klement, P.; Jones, A.; Ghimire, N.; Yan, J. Q.; Mandrus, D.; Taniguchi, T.; Watanabe, K.; Kitamura, K.; Yao, W.; Cobden, D.; Xu, X. Electrically tunable excitonic light-emitting diodes based on monolayer WSe_2 p−n junctions. *Nat. Nanotechnol.* **2014**, *9*, 268−272.
(14) Mak, K. F.; He, K.; Lee, C.; Lee, G.; Hone, J.; Heinz, T. F.; Shan, J. Tightly bound trions in monolayer MoS_2. *Nat. Mater.* **2013**, *12* (3), 207−211.
(15) Lien, D.; Uddin, S. Z.; Yeh, M.; Amani, M.; Kim, H.; Ager, J. W.; Yablonovitch, E.; Javey, A. Electrical suppression of all nonradiative recombination pathways in monolayer semiconductors. *Science* **2019**, *364* (6439), 468−471.
(16) Cao, Y.; Rodan-Legrain, D.; Rubies-Bigorda, O.; Park, J. M.; Watanabe, K.; Taniguchi, T.; Jarillo-Herrero, P. Tunable correlated states and spin-polarized phases in twisted bilayer−bilayer graphene. *Nature* **2020**, *583* (7815), 215−220.
(17) Rivera, P.; Schaibley, J. R.; Jones, A. M.; Ross, J. S.; Wu, S.; Aivazian, G.; Klement, P.; Seyler, K.; Clark, G.; Ghimire, N. J.; Yan, J.; Mandrus, D. G.; Yao, W.; Xu, X. Observation of long-lived interlayer excitons in monolayer $MoSe_2$−WSe_2 heterostructures. *Nat. Commun.* **2015**, *6* (1), 6242.
(18) Dean, C. R.; Wang, L.; Maher, P.; Forsythe, C.; Ghahari, F.; Gao, Y.; Katoch, J.; Ishigami, M.; Moon, P.; Koshino, M.; Taniguchi, T.; Watanabe, K.; Shepard, K. L.; Hone, J.; Kim, P. Hofstadter's butterfly and the fractal quantum Hall effect in moiré superlattices. *Nature* **2013**, *497* (7451), 598−602.
(19) Kang, K.; Lee, K.-H.; Han, Y.; Gao, H.; Xie, S.; Muller, D. A.; Park, J. Layer-by-layer assembly of two-dimensional materials into wafer-scale heterostructures. *Nature* **2017**, *550* (7675), 229−233.
(20) Seyler, K. L.; Rivera, P.; Yu, H.; Wilson, N. P.; Ray, E. L.; Mandrus, D. G.; Yan, J.; Yao, W.; Xu, X. Signatures of moire-trapped valley excitons in $MoSe_2$/WSe_2 heterobilayers. *Nature* **2019**, *567* (7746), 66−70.
(21) Alexeev, E. M.; Ruiz-Tijerina, D. A.; Danovich, M.; Hamer, M. J.; Terry, D. J.; Nayak, P. K.; Ahn, S.; Pak, S.; Lee, J.; Sohn, J. I.; Molas, M. R.; Koperski, M.; Watanabe, K.; Taniguchi, T.; Novoselov, K. S.; Gorbachev, R. V.; Shin, H. S.; Fal'ko, V. I.; Tartakovskii, A. I. Resonantly hybridized excitons in moire superlattices in van der Waals heterostructures. *Nature* **2019**, *567* (7746), 81−86.
(22) Jin, C.; Regan, E. C.; Yan, A.; Utama, M. I. B.; Wang, D.; Zhao, S.; Qin, Y.; Yang, S.; Zheng, Z.; Shi, S.; Watanabe, K.; Taniguchi, T.; Tongay, S.; Zettl, A.; Wang, F. Observation of moiré excitons in WSe_2/WS_2 heterostructure superlattices. *Nature* **2019**, *567* (7746), 76−80.
(23) Tran, K.; Moody, G.; Wu, F.; Lu, X.; Choi, J.; Kim, K.; Rai, A.; Sanchez, D. A.; Quan, J.; Singh, A.; Embley, J.; Zepeda, A.; Campbell, M.; Autry, T.; Taniguchi, T.; Watanabe, K.; Lu, N.; Banerjee, S. K.; Silverman, K. L.; Kim, S.; Tutuc, E.; Yang, L.; MacDonald, A. H.; Li, X. Evidence for moiré excitons in van der Waals heterostructures. *Nature* **2019**, *567* (7746), 71−75.
(24) Cao, Y.; Fatemi, V.; Fang, S.; Watanabe, K.; Taniguchi, T.; Kaxiras, E.; Jarillo-Herrero, P. Unconventional superconductivity in magic-angle graphene superlattices. *Nature* **2018**, *556* (7699), 43−50.
(25) Xu, W.; Liu, W. T.; Schmidt, J. F.; Zhao, W.; Lu, X.; Raab, T.; Diederichs, C.; Gao, W.; Seletskiy, D. V.; Xiong, Q. Correlated fluorescence blinking in two-dimensional semiconductor heterostructures. *Nature* **2017**, *541* (1), 62−67.
(26) Godiksen, R. H.; Wang, S.; Raziman, T. V.; Guimaraes, M. H. D.; Rivas, J. G.; Curto, A. G. Correlated exciton fluctuations in a two-dimensional semiconductor on a metal. *Nano Lett.* **2020**, *20* (7), 4829−4836.
(27) Marcus, R. A. Electron transfer reactions in chemistry: theory and experiment (Nobel Lecture). *Angew. Chem. Int. Ed. Engl.* **1993**, *32* (8), 1111−1121.
(28) Jin, C.; Ma, E. Y.; Karni, O.; Regan, E. C.; Wang, F.; Heinz, T. F. Ultrafast dynamics in van der Waals heterostructures. *Nat. Nanotechnol.* **2018**, *13* (11), 994−1003.
(29) Qiu, H.; Xu, T.; Wang, Z.; Ren, W.; Nan, H.; Ni, Z.; Chen, Q.; Yuan, S.; Miao, F.; Song, F.; Long, G.; Shi, Y.; Sun, L.; Wang, J.; Wang, X. Hopping transport through defect-induced localized states in molybdenum disulphide. *Nat. Commun.* **2013**, *4*, 2642.
(30) Hong, X.; Kim, J.; Shi, S.-F.; Zhang, Y.; Jin, C.; Sun, Y.; Tongay, S.; Wu, J.; Zhang, Y. F.; Wang, F. Ultrafast charge transfer in atomically thin MoS_2/WS_2 heterostructures. *Nat. Nanotechnol.* **2014**, *9*, 682−686.
(31) Wu, L.; Chen, Y.; Zhou, H.; Zhu, H. Ultrafast energy transfer of both bright and dark excitons in 2D van der Waals heterostructures beyond dipolar coupling. *ACS Nano* **2019**, *13* (2), 2341−2348.
(32) Kozawa, D.; Carvalho, A.; Verzhbitskiy, I.; Giustiniano, F.; Miyauchi, Y.; Mouri, S.; Castro Neto, A. H.; Matsuda, K.; Eda, G. Evidence for fast interlayer energy transfer in $MoSe_2$/WS_2 heterostructures. *Nano Lett.* **2016**, *16* (7), 4087−4093.
(33) Long, R.; Prezhdo, O. V. Quantum coherence facilitates efficient charge separation at a MoS_2/$MoSe_2$ van der Waals junction. *Nano Lett.* **2016**, *16* (3), 1996−2003.
(34) Zereshki, P.; Wei, Y.; Long, R.; Zhao, H. Layer-coupled states facilitate ultrafast charge transfer in a transition metal dichalcogenide trilayer heterostructure. *J. Phys. Chem. Lett.* **2018**, *9* (20), 5970−5978.
(35) Wang, Y.; Wang, Z.; Yao, W.; Liu, G.-B.; Yu, H. Interlayer coupling in commensurate and incommensurate bilayer structures of transition metal dichalcogenides. *Phys. Rev. B: Condens. Matter Mater. Phys.* **2017**, *95*, 115429−115441.

https://doi.org/10.1021/acs.nanolett.1c01356
Nano Lett. 2021, 21, 6773−6780